



You Don't Need Reproducible Research

# UNTIL YOU DO.

If your work is successful in your lab, it should be successful on the other side of the world. That's why we engineer CO<sub>2</sub>/O<sub>2</sub> incubators that deliver reproducible results, contamination free and equal to *in vivo* reality.

Minimize uncertainty  
with PHCbi brand products



## PHC Corporation of North America

PHC Corporation of North America  
1300 Michael Drive, Suite A, Wood Dale, IL 60191  
Toll Free USA (800) 858-8442, Fax (630) 238-0074  
[www.phchd.com/us/biomedical](http://www.phchd.com/us/biomedical)

[phchd.com/us/biomedical/cell-culture-incubators](http://phchd.com/us/biomedical/cell-culture-incubators)

PHC Corporation of North America is a subsidiary of PHC Holdings Corporation, Tokyo, Japan, a global leader in development, design and manufacturing of laboratory equipment for biopharmaceutical, life sciences, academic, healthcare and government markets.

**Life Science Innovator Since 1966**

## ARTICLE

# Development of a rapid polarized total synchronous fluorescence spectroscopy (pTSFS) method for protein quantification in a model bioreactor broth

Bernard O. Boateng  | Saioa Elcoroaristizabal  | Alan G. Ryder 

Nanoscale BioPhotonics Laboratory, School of Chemistry, National University of Ireland, Galway, Ireland

**Correspondence**

Alan G. Ryder, Nanoscale BioPhotonics Laboratory, School of Chemistry, National University of Ireland, Galway H91 CF50, Ireland.  
Email: [alan.ryder@nuigalway.ie](mailto:alan.ryder@nuigalway.ie)

**Funding information**

Science Foundation Ireland, Grant/Award Numbers: 14/IA/2282, Advanced Analytics for Biological Therapeutic Manufacture; European Regional Development Fund, Grant/Award Numbers: 14/IA/2282, Advanced Analytics for Biological Therapeutic Manufacture.

**Abstract**

Protein quantification during bioprocess monitoring is essential for biopharmaceutical manufacturing and is complicated by the complex chemical composition of the bioreactor broth. Here we present the early-stage development and optimization of a polarized total synchronous fluorescence spectroscopy (pTSFS) method for protein quantification in a hydrolysate-protein model (mimics clarified bioreactor broth samples) using a standard benchtop laboratory fluorometer. We used UV transmitting polarizers to provide wider range pTSFS spectra for screening of the four different TSFS spectra generated by the measurement: parallel ( $\parallel$ ), perpendicular ( $\perp$ ), unpolarized (T) intensity spectra and anisotropy maps. TSFS $_{\parallel}$  (parallel polarized) measurements were the best for protein quantification compared to standard unpolarized measurements and the Bradford assay. This was because TSFS $_{\parallel}$  spectra had a better analyte signal to noise ratio (SNR), due to the anisotropy of protein emission. This meant that protein signals were better resolved from the background emission of small molecule fluorophores in the cell culture media. SNR of  $>5000$  was achieved for concentrations of bovine serum albumin/yeastolate  $1.2/10 \text{ g L}^{-1}$  with TSFS $_{\parallel}$ . Optimization using genetic algorithm and interval partial least squares based variable selection enabled reduction of spectral resolution and number of excitation wavelengths required without degrading performance. This enables fast ( $<3.5 \text{ min}$ ) online/at-line measurements, and the method had an LOD of  $0.18 \text{ g L}^{-1}$  and high accuracy with a predictive error of  $<9\%$ .

**KEYWORDS**

bioprocess monitoring, chemometrics, multidimensional fluorescence, polarization, process analytical technology, protein

## 1 | INTRODUCTION

Bioprocess monitoring is important in ensuring high productivity manufacturing of therapeutic proteins. Accurate protein quantification during industrial cell culture is considered as one of the most important critical process parameters that needs to be measured for upstream process control (Rathore & Winkle, 2009). This calls for fast, accurate, and robust analytical methods capable of real-time

monitoring of biologic protein production in accordance with the process analytical technology (PAT) and quality by design (QbD) initiatives. During cell culture processes, protein product concentration increases as the process progresses from very low to relatively high concentrations. The matrix in which the protein is produced is also very chemically and physically complex which continually evolves. Cell culture media (Gronemeyer et al., 2014) contains amino acids, sugars, salts, and other small to medium-sized molecules,

This is an open access article under the terms of the Creative Commons Attribution License, which permits use, distribution and reproduction in any medium, provided the original work is properly cited.

© 2021 The Authors. *Biotechnology and Bioengineering* Published by Wiley Periodicals LLC

which change as the cells metabolize these nutrients. Furthermore, the presence of host cell proteins, whole cells, and cell debris, produces a solution with continually varying physical properties. All these factors can severely limit the application of many conventional methods for protein quantification.

There are a variety of methods which can measure the total protein content, or quantify a single protein type, or determine multiple proteins simultaneously (Chutipongtanate et al., 2012). Total protein quantitation usually relies on traditional colorimetric methods such as Bradford, Lowry, and Bicinchoninic acid (BCA) assays (Bradford, 1976; Smith et al., 1985), but these are more suitable for low protein concentrations ( $10\text{--}2000\ \mu\text{g ml}^{-1}$ ). Detection of specific proteins within complex mixtures are usually performed by enzyme-linked immunosorbent assay and western blot analysis, however, they usually have low accuracy and precision (Walker, 1996). More accurate methods include mass spectrometry based techniques (Reusch et al., 2015), however, these require extensive sample preparation which can be problematic to integrate into manufacturing to enable online or in-line measurements required for rapid, real-time analysis. Spectroscopic techniques, like ultraviolet-visible (UV-vis) absorbance (Classen et al., 2017), near infrared (NIR) and mid-infrared (MIR) absorption (Cervera et al., 2009; Hakemeyer et al., 2013; Jose et al., 2011), and Raman scattering (B. Li et al., 2013), are noninvasive, non-destructive, fast methods capable of on-line protein content monitoring. UV-vis absorbance spectroscopy is fast and inexpensive, but it usually lacks the required sensitivity and specificity. MIR and NIR, are more informative, but very sensitive to the presence of polar compounds and water (Ryder, 2018). Water contamination is less of an issue for Raman spectroscopy, which facilitates its use for bioprocess monitoring in solution (Buckley & Ryder, 2017). However, the sensitivity of the method is limited by the weak protein spectra from bioprocess broths (B. Li et al., 2013), background scatter, and fluorescence interference (Buckley & Ryder, 2017).

Fluorescence spectroscopy has several advantages for protein analysis in bioprocess monitoring: proteins have intrinsic fluorescence that can be discriminated from other fluorophores, it is non-destructive, offers fast measurements, relatively inexpensive, can require no sample handling and can be applied in either in-line or at-line (Calvet et al., 2014; Groza et al., 2014; B. Li et al., 2014; Teixeira et al., 2011). These characteristics meet the criteria for the development of a PAT (Rathore et al., 2010; Read et al., 2010) in line with QbD principles for biopharmaceutical manufacturing (Rathore & Winkle, 2009). However, using single excitation wavelength fluorescence spectra limits the ability to resolve analyte fluorophores from strong background signals as is the case with bioreactor monitoring. Multidimensional fluorescence (MDF) measurements generate more unique fingerprints of protein emission which comprises the overlapped spectra of intrinsically fluorescent amino acids, mostly tryptophan (Trp) and tyrosine (Tyr). Phenylalanine is also fluorescent but it has a very low quantum yield (0.02) and if incorporated in proteins tends to undergo Förster resonance energy transfer (FRET) to Trp and Tyr (Lakowicz, 2006) and is thus rarely

observed in proteins or complex mixtures. There are two complications with bioprocess monitoring by fluorescence spectroscopy which also need to be taken into consideration. First the population of small molecule fluorophores from the media and fluorescent metabolites produced will change very significantly during the process, contributing to a varying background interference signal. Second, the presence of fluorescent host cell proteins will also contribute to the fluorescence emission in the same regions as the product protein. However, despite this we have in the past shown that excitation-emission matrix (EEM) can be used to quantitatively model process performance in the presence of all these interfering signals (B. Li et al., 2014).

MDF measurements can be made as an EEM or as a total synchronous fluorescence scan (TSFS) with most scanning-based spectrometers. One TSFS advantage is being able to avoid the collection of Rayleigh scatter as observed in EEM spectra, and this can assist in ensuring more accurate anisotropy measurements because scattered light is highly polarized. With polarized fluorescence spectroscopy, one can exploit the intrinsic protein emission anisotropy to achieve better resolution by discriminating the protein emission from that of the small molecule fluorophores in culture media or bioreactors. The anisotropy of protein emission arises from the slower rate of rotational diffusion which is largely due to their much larger sizes (Lakowicz, 2006). However, multiple other factors such as the physicochemical environment, the presence of quenchers, and FRET also affect anisotropy, making this a multivariate analysis problem. Using anisotropy measurements we demonstrated previously the ability to accurately quantify protein content ( $0.1\text{--}4\ \text{g L}^{-1}$ ) in solutions with fixed media concentration (Groza et al., 2014). However, full spectrum anisotropy-based measurements are slower, and noisier, than simple intensity-based measurements, making it a less suitable PAT option for dynamic and complex bioprocesses (B. Li et al., 2014; Ryan et al., 2010). Some of the advantages and disadvantages of multidimensional fluorescence spectroscopy are summarized in Tables S1).

MDF measurements and chemometrics have been widely applied to bioprocess monitoring such as the production of monoclonal antibodies (Ohadi et al., 2015; Schwab et al., 2016), antigens (Zavatti et al., 2016), and the quality control of cell culture media (Calvet et al., 2014; B. Li et al., 2011; Ryan et al., 2010). Still, MDF measurements generate large amount of spectral data that require careful interpretation and data reduction while retaining the essential information, which is generally accomplished using chemometric multivariate analysis tools. Curve resolution methods like PARALLEL FACTOR analysis (PARAFAC; Elcoroaristizabal et al., 2015; Murphy et al., 2013) or multivariate curve resolution-alternating least squares (MCR-ALS; Casamayou-Boucau & Ryder, 2018; de Juan et al., 2014) can sometimes resolve the analyte of interest spectrum, from the background or interferents, but they are generally subjected to significant matrix effects in complex, biogenic solutions. Multivariate regression methods like unfolded (U-PLS) or N-way partial least squares (N-PLS) usually provide better predictive performance, but they have problems where the relationship between

signal and concentration is very nonlinear such as in bioreactors (Olivieri, 2018). This nonlinearity is caused by multiple factors including: high spectral overlap, primary and secondary inner filter effects (IFE), FRET, and noise (Ghisaidoobe & Chung, 2014). Non-linear multivariate regression methods like artificial neural networks (ANN) may be more suitable (Chiappini et al., 2020; Melcher et al., 2015), but these are more complex, do not provide spectral information, and are more prone to overfitting when only a limited number of samples/concentration range is available (Despagne et al., 2000). MDF spectra also generally contain a lot of both uninformative nonfluorescent spectral variables and highly correlated spectral variables (where there is emission) that should be removed as these can decrease robustness and increase model error. There are many variable selection methods described in the literature of which three of the most common methods are variable importance in projection (VIP; Svante Wold et al., 2002), interval partial least squares (iPLS; Nørgaard et al., 2000), and Genetic Algorithm (GA; Leardi et al., 2002).

Here, we investigate the efficacy of polarized TSFS (pTSFS) measurements using a standard laboratory benchtop spectrometer for protein quantification in a model bioreactor broth comprising of bovine serum albumin (BSA) and yeastolate (YST; water soluble extract of autolysed yeast), using UV transmitting wire grid polarisers (WGP; Casamayou-Boucau & Ryder, 2017). WGP enable the measurement of tyrosine emission ( $\lambda_{\text{ex}} = 275\text{--}280\text{ nm}$ ), in comparison with the previously used thin film polarisers (Groza et al., 2014). Furthermore, we compare the efficacy of polarized (parallel and perpendicular) to unpolarized spectra and anisotropy maps in terms of their analytical (qualitative and quantitative) performance. To further improve protein quantification we investigated design of experiments (DoE) approaches (Anderson-Cook et al., 2009) for instrumental optimization and variable selection for data and spectra optimization. This test system was designed to provide foundation level data about the efficacy of this measurement method, before progressing to the analysis of samples from real industrial bioprocesses. The long-term goal of this study is to produce a rapid, accurate, and robust quantification methodology for eventual on- or at-line protein quantification suitable for industrial use.

## 2 | MATERIALS AND METHODS

### 2.1 | Materials and samples

Yeastolate ultra-filtered (UF, 10 kDa molecular weight cut-off) was obtained from Becton Dickson and used as received. BSA (>99%, lyophilized powder, globulin free), Bradford reagent (product number B6916), and phosphate buffered saline (PBS) tablets were from Sigma-Aldrich (Merck). HPLC grade water (Honeywell) was used for PBS stock solutions preparation. All materials and reagents were used without further purification. Yeastolate ( $50\text{ g L}^{-1}$ ) and BSA ( $5\text{ g L}^{-1}$ ) stock solutions were prepared in PBS buffer ( $\text{pH } 7.4 \pm 0.01$ ) and then membrane filtered ( $0.22\ \mu\text{m}$ ). Three samples sets were

prepared: Calibration set (C-Set), a Test set (T-Set), and an instrumental optimization set (IO-Set). The C-Set comprised of 15 different mixtures, prepared in triplicate ( $n = 45$ ) and was based on a D-optimal factorial design with: yeastolate concentration ranges:  $9.0\text{--}11.0\text{ g L}^{-1}$  ( $n = 3$ ,  $\Delta c = 1\text{ g L}^{-1}$ ) and  $0.4\text{--}1.2\text{ g L}^{-1}$  for BSA ( $n = 5$ ,  $\Delta c = 0.2\text{ g L}^{-1}$ ). A three level yeastolate concentration was selected to simulate the changing fluorescence emission as the cell culture evolves during a bioprocess. This BSA concentration was selected as being representative of titer values for monoclonal antibody production (Shukla et al., 2017). Difference plots of the normalized yeastolate spectra at these concentrations show changes in spectral shape at long excitation wavelengths (320–380 nm) due to IFE. These changes in fluorescence intensity and spectral shape (Figure S1, SI) are characteristic of the spectral changes experienced during mammalian cell culture (B. Li et al., 2014). The external validation set (T-Set) comprised of 6 mixtures, prepared in triplicate ( $n = 18$ ) with BSA concentration ranging from  $0.5$  to  $0.9\text{ g L}^{-1}$  ( $n = 3$ ,  $\Delta c = 0.2\text{ g L}^{-1}$ ) and yeastolate at  $10$  and  $11\text{ g L}^{-1}$  ( $n = 2$ ,  $\Delta c = 1\text{ g L}^{-1}$ ). The simple IO-Set used a fixed  $10\text{ g L}^{-1}$  yeastolate concentration with low ( $0.4\text{ g L}^{-1}$ ) and high ( $1.2\text{ g L}^{-1}$ ) BSA concentrations. Aliquots of each sample were dispensed into 2 ml Lobind tubes (Eppendorf) and stored at  $-70^\circ\text{C}$  before use (over 3 weeks) to limit compositional changes. Before analysis, samples were defrosted overnight at  $2\text{--}8^\circ\text{C}$  and checked for ice particles before use. This procedure was used to minimize preparation variation and ensure that all samples had the same freeze-thaw profile. Aseptic solution preparation was carried out in a laminar flow hood to minimize contamination. The Bradford assay was selected as a simple orthogonal method (Bradford, 1976) to validate the performance of the fluorescence spectroscopy based predictive models and experimental details are provided in the Supporting Information (SI).

### 2.2 | Instrumentation and data collection

Absorbance spectra were measured along the short cuvette axis using an Agilent Cary 60 UV-Vis (Agilent Technologies) spectrophotometer with corresponding PBS stock solutions as reference. TSFS spectra were collected using a modified Cary Eclipse fluorometer (Agilent Technologies) fitted with polarizers and temperature control. Instrument settings were similar to that reported elsewhere (Steiner-Browne et al., 2019) and details are given in the SI.

### 2.3 | Data analysis

Chemometric data analysis was performed using the PLS\_Toolbox ver. 8.2.1 (Eigenvector Research Inc.) working in a MATLAB environment ver. 9.1.0 (The Mathworks Inc.) and in-house written codes. Experimental design and analysis were performed using Minitab Statistical Software ver. 17 (Minitab Inc.). Full details of data pretreatment and MCR modelling is provided in the SI. BSA

quantification was done using partial least squares (PLSs) regression (S. Wold et al., 2001) in the unfolded (U-PLS; Geladi, 2002) configuration. Different pre-processing methods were evaluated including normalization and mean-centering. The optimum number of latent variables (LVs) was estimated during leave-one-out cross-validation by comparing the root-mean-square error of calibration (RMSEC) and cross-validation (RMSECV; Olivieri, 2018) as a function of the number of LV, and the F-ratio criterion (Haaland & Thomas, 1988). The Durbin-Watson test (Olivieri, 2018) was used to verify the model non-linearities. For intensity-based methods, spectral normalization (to maximum intensity) was necessary to ensure PLS model linearity (Table S6, SI), consequently all models were built using blank subtracted, normalized data. No spectral pretreatment was required or implemented for *aniso*-TSFS data.

Model performance was evaluated using the external validation test set (T-set) based on determination coefficients ( $R^2$ ), root-mean-square error of prediction (RMSEP), and relative (to the mean value) error of prediction (REP). RMSEP gives an average error of the predicted BSA concentration in  $\text{g L}^{-1}$  (Næs et al., 2002). Accuracy and precision of the different methods were compared using the Elliptical Joint Confidence Region test (EJCR; Mandel & Linning, 1957). The EJCR was calculated to evaluate the slope and the intercept of the regression of the reference and predicted values at a 95% confidence interval. If the 1,0 point is inside the EJCR, it can be concluded that constant and proportional biases were absent. Evaluation of significant differences between the predictive accuracy of the methods was also tested using a randomization test (van der Voet, 1994).

## 2.4 | Variable selection

PLS model robustness and accuracy for quantitative analysis can be improved using variable selection, to reduce the influence of uninformative and/or nonlinear spectral data (Odman et al., 2010). Details of VIP, iPLS, and GA methods used are in the SI.

## 2.5 | Instrument optimization

Response surface methodology (Jensen, 2017) was used to determine the optimum instrumental parameters that maximizes the signal quality, signal to noise ratio (SNR) of the spectrally optimized TSFS<sub>||</sub> measurements evaluated at two BSA concentrations (IO-Set). SNR was determined by the ratio of the average maximum BSA signal and the standard deviation of the noise determined by a selected area in the spectra with no fluorescence signal (Figure S2, SI) and mathematically calculated using the formula in reference (Skoog, 1976). The influence of the emission bandwidth (2.5/5/10 nm), scan rate (120/1200/2400  $\text{nm min}^{-1}$ ), and PMT voltage (600/650/700 V) on SNR was examined using a Box Behnken design (Anderson-Cook et al., 2009). The design consisted of 15 test conditions with three levels per instrumental factor and was tested at

the lowest and highest BSA concentration conditions (0.4 and  $1.2 \text{ g L}^{-1}$  of BSA in  $10 \text{ g L}^{-1}$  yeastolate). The order of experiments was randomized to avoid bias. A composite desirability function was used to determine the optimal instrumental settings. The individual desirability ( $d$ ) evaluates how the settings optimize each single response (SNR at each BSA concentration level), whereas the composite desirability ( $D$ ) defines the settings that optimize both responses (at two BSA concentrations). A value of one for the desirability function indicates the ideal optimization (Derringer & Suich, 1980).

## 3 | RESULTS AND DISCUSSION

The yeastolate-protein model system used here was selected primarily as a model to facilitate measurement and data analysis method development using a chemically complex sample system. This system was designed to simulate the chemical and optical complexity of clarified reactor broth samples. Clarified broth solutions are samples extracted from a bioreactor which have been filtered or processed to remove whole cells and the large cell fragments. Furthermore, yeastolate and BSA are also inexpensive, facilitating the generation of large sample sets and replicate measurements, thus making it easy for laboratories everywhere to easily prepare these samples and thus accurately compare the performance of different analytical techniques without the need to undertake costly, and irreproducible cell culture processes. To replicate a real, unclarified, bioprocess broth solution would require the addition of particulate matter to replicate the scatter due to whole cells and cell fragments. This we feel is outside the scope of the present study, as it requires significant input from multiple sources (e.g., academia, industry, and standards agencies) to achieve consensus as to how a practical model system can be defined. An issue with developing new analytical methods is that if one uses real processes then it is difficult to replicate the measurements and compare measurement efficacy with data collected from widely differing bioprocesses (e.g., *Escherichia coli* fermentation and CHO mammalian cell culture). It should be noted that there are no defined standard bioprocess sample systems described in the literature, whereas in biomedical spectroscopy, an area of high optical complexity, for example, the use of tissue phantoms is well established, and standards agencies such as NIST are heavily involved (Lemaitte et al., 2016). Here, a relatively low protein concentration range was selected as this is the range where quantification is more difficult (B. Li et al., 2014), particularly for the early bioprocess stages, and we wished to be able to compare efficacy with a previous study (Groza et al., 2014).

### 3.1 | Spectral analysis

The model culture media and calibration set samples all have a very strong absorbance in the UV ( $A_{280} > 3$  a.u. for C-Set, Figure S3, SI) because of overlap between the absorbance of the protein and cell

culture media components like amino acids which are present in relatively high concentrations, similar to that of clarified industrial bioprocess broths. This effectively prevents the use of absorbance spectroscopy as a quantitative method for in-process protein analysis. This high absorbance also causes very strong IFE, which has a significant impact on UV fluorescence (Ryder et al., 2017).

BSA intrinsic emission ( $\lambda_{\text{ex}} = 285\text{--}300\text{ nm}$ , Figure 1) mostly originates from Trp with a relatively small Tyr contribution and even less from phenylalanine, largely because of FRET processes (Lakowicz, 2006). Intrinsic yeastolate emission (and most cell culture media) is more complex because of the large number of small molecule fluorophores present. The emission can be split into three main regions (Figures 1 and S4, SI): R1 ( $\lambda_{\text{ex}} = 240\text{--}300\text{ nm}$ ) mostly related to emission from aromatic amino acids (B. Y. Li et al., 2012); R2 ( $\lambda_{\text{ex}} = 320\text{--}360\text{ nm}$ ) corresponding to larger fluorophores such as vitamins (Faassen & Hitzmann, 2015), and R3 ( $\lambda_{\text{ex}} > 360\text{ nm}$ ) corresponding to co-factors and flavins (Graf et al., 2019). The strong yeastolate and BSA spectral overlap (Figure 1, R1) coupled with the presence of multiple chemical constituents from yeastolate, like paramagnetic ions, histidine (Lakowicz, 2006), and also non-emitting chromophores (B. Li et al., 2010), significantly reduces BSA emission intensity through quenching and IFE processes. For instance, when the BSA ( $1\text{ g L}^{-1}$ ) spectrum was compared to a  $1:10\text{ g L}^{-1}$  mixture, BSA emission intensity decreased by 58% (TSFS<sub>||</sub>), >53% (TSFS<sub>T</sub>), and by >50% for TSFS<sub>⊥</sub> (Table S2, SI). The stronger quenching of protein emission observed in TSFS<sub>||</sub> was due to higher IFE sensitivity and the small additional scattering contributions in these spectra. Furthermore, the intensity changes were nonlinear (Figure S4, SI), which makes univariate-based quantitation difficult.

Comparison of polarization modes (Figures S5–S8 and Table S2, SI), verified that the parallel polarization was more sensitive to protein emission, with the BSA/YST ratio (calculated as the ratio of the  $1\text{ g L}^{-1}$  BSA in buffer signal of to that of  $10\text{ g L}^{-1}$  YST) in pure solutions of  $1.13$  (TSFS<sub>||</sub>) >  $0.99$  (TSFS<sub>T</sub>) >  $0.93$  (TSFS<sub>⊥</sub>). Despite TSFS<sub>T</sub> measurements having the strongest absolute protein emission signal, the matrix contribution is also the highest leading to a poorer protein signal to matrix ratio (BSA signal to BSA/YST matrix ratio,<sup>1</sup> which was highest for (TSFS<sub>||</sub>) =  $1.02 > \text{TSFS}_T$  ( $0.92$ ) > TSFS<sub>⊥</sub> ( $0.86$ ). The changes in fluorescence intensity between C-Set samples were more pronounced in the tryptophan emission region of and in the TSFS<sub>||</sub> spectra. This suggests that the parallel polarization measurement is potentially more sensitive to changes in protein emission signal. The repeatability and intermediate precision of replicate pTSFS measurements were all acceptable, with RSD values of <1% and ≈5%, respectively (Tables S3 and S4, SI). BSA has maximum anisotropy, ~0.22 at  $\lambda_{\text{ex}}/\Delta\lambda = 310\text{ nm}/40\text{--}60\text{ nm}$  ( $\lambda_{\text{em}} = 350\text{--}360\text{ nm}$ ), however, this varies very significantly across the emission space because of a combination of FRET and environmental effects (Lakowicz, 2006). These data agree with literature value of  $0.219 \pm 0.002$  ( $\lambda_{\text{ex}}/\lambda_{\text{em}} = 340/470\text{ nm}$ , 20°C) recorded using dansyl

labelled BSA (Flecha & Levi, 2003), and intrinsic emission measurements,  $\lambda_{\text{ex}}/\lambda_{\text{em}} = 294\text{--}305/324\text{--}363\text{ nm}$  (Groza et al., 2014).

### 3.2 | Deep UV MDF spectral features observed

Using WGP instead of standard thin film polarisers (TFP) enabled UV excitation below 280 nm. This led to slight changes in the shape and anisotropy profile of a similar model system studied previously (Groza et al., 2014). Excitation below 280 nm allowed for more light absorption by Tyr resulting in higher emission from both Tyr and Trp with additional emission from Trp (via hetero-FRET) and Tyr (via homo-FRET). There are also differences observed in the TSFS spectra obtained with WGP in comparison to that obtained with TFP. For TFP and WGP collected spectra, the most polarized emission for BSA occurred at  $\lambda_{\text{ex}}/\lambda_{\text{em}} = 300/340$  and  $280\text{--}295/340\text{ nm}$ , respectively. This blue shift corresponds to increased Tyr emission which is important for proteins that lack a Trp residue such as Insulin (Casamayou-Boucau & Ryder, 2020). As previously, *aniso*-TSFS maps (Figure 1) of yeastolate shows almost negligible anisotropy, except for the free amino acid emission region (R1)  $r = .01 \pm 0.003$  and a small contribution from Raman scatter. However, this contribution was significantly lower (<10%) than the protein anisotropy component which shows the increased selectivity of using anisotropy measurements. The high anisotropy of protein emission is reduced in mixtures (Figure 1) because of emission overlap with yeastolate, and multiple depolarization factors such as energy transfer, IFE, quenching and possible binding processes (Lakowicz, 2006). In the long wavelength region, R3 ( $\lambda_{\text{ex}}/\Delta\lambda = 350\text{--}376/100\text{--}140\text{ nm}$ ), where emission was dominated by yeastolate, a small increase in anisotropy (average  $r = .03 \pm 0.001$ ) was also observed with increasing BSA concentration. This may indicate binding of small molecule fluorophores from yeastolate with BSA (Groza et al., 2014; Naveenraj & Anandan, 2013). However, reproducibility (RSD = 15%–20%) and repeatability values (RSD = 4.0%–5.4%) for *aniso*-TSFS (Tables S3 and S4, SI) were worse, due to the error propagation associated with calculating anisotropy from multiple spectral measurements. This along with the long analysis time required, made *aniso*-TSFS measurements a less viable PAT option, and as such we now focus on pTSFS measurements.

### 3.3 | Qualitative analysis

MCR-ALS (Table 1) was used to identify the origin of the different pTSFS spectral changes. A two component MCR model, C1 (yeastolate emission) and C2 (BSA emission), showed that TSFS<sub>||</sub> was more sensitive to BSA emission than the other configurations (with 14.43%, 11.12%, and 12.25% of the variance explained in TSFS<sub>||</sub>, TSFS<sub>⊥</sub>, and TSFS<sub>T</sub> modes, respectively). This 12% increase in BSA emission intensity compared to the conventional TSFS<sub>T</sub> measurement was significant for quantitative analysis. However, singular value decomposition (SVD) analysis indicated that a four-component

<sup>1</sup>This was calculated as the ratio of BSA ( $1\text{ g L}^{-1}$  in buffer) emission intensity to the signal from a mixture of BSA ( $1\text{ g L}^{-1}$ ) in yeastolate ( $10\text{ g L}^{-1}$ ).

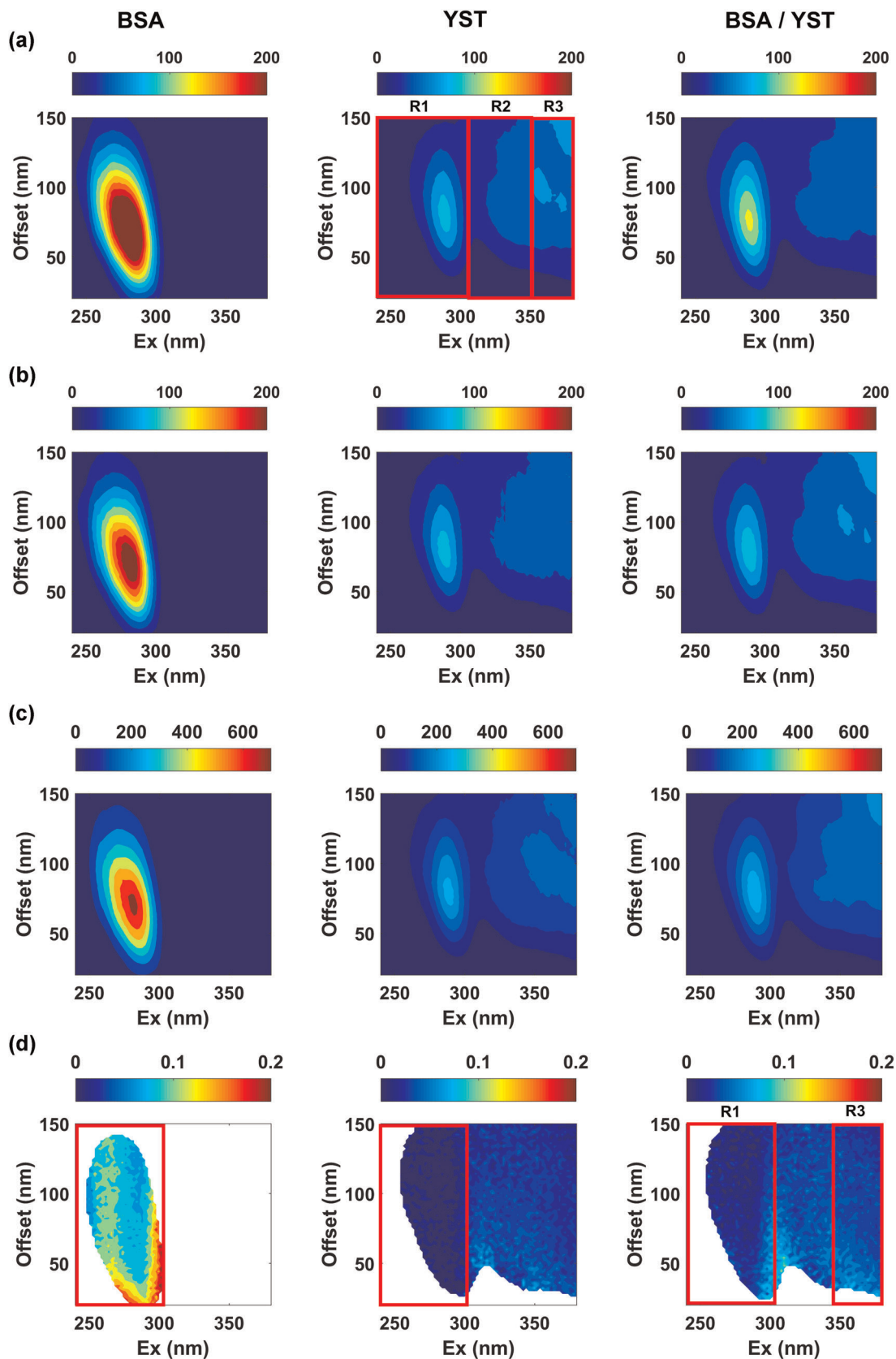


**FIGURE 1** (a) TSFS<sub>B</sub>, (b) TSFS<sub>L</sub>, (c) TSFS<sub>T</sub>, and (d) aniso-TSFS maps of: (left) BSA 1 g L<sup>-1</sup>, (middle) yeastolate 10 g L<sup>-1</sup>, and (right) BSA/yeastolate in a 1.0/10 g L<sup>-1</sup> mixture. BSA, bovine serum albumin; TSFS, total synchronous fluorescence spectroscopy; YST, yeastolate [Color figure can be viewed at [wileyonlinelibrary.com](http://wileyonlinelibrary.com)]

**TABLE 1** Comparison of the MCR model parameters and components obtained for the intensity-based MDF methods

Configuration	Component	LOF (%)	Variance explained (%)	Siml	$\lambda_{ex}/\Delta\lambda$ (nm)
Two component MCR models					
TSFS <sub>  </sub>	C1 (YST)		85.4	0.88	290/78
	C2 (BSA)		14.4	0.97	282/70
	Model	3.7	99.9		
TSFS <sub>⊥</sub>	C1 (YST)		88.8	0.90	290/78
	C2 (BSA)		11.1	0.96	280/74
	Model	3.6	99.9		
TSFS <sub>T</sub>	C1 (YST)		87.6	0.90	290/78
	C2 (BSA)		12.3	0.97	280/74
	Model	3.6	99.9		
Four component MCR models					
TSFS <sub>  </sub>	C1 (YST)		84.1	0.99	290/82
	C2 (BSA)		11.8	0.73	282/70
	C3		2.9		290/70
	C4		1.2		280/80
	Model	1.08	99.9		
TSFS <sub>⊥</sub>	C1 (YST)		89.2	0.99	290/80
	C2 (BSA)		7.0	0.89	280/74
	C3		2.1		378/136
	C4		1.8		286/60
	Model	3.30	99.9		
TSFS <sub>T</sub>	C1 (YST)		88.1	0.99	290/80
	C2 (BSA)		8.2	0.88	280/74
	C3		1.9		378/136
	C4		1.7		288/60
	Model	3.16	99.9		

Note: LOF and Siml represent the lack of fit and similarity index, respectively. Siml was calculated for C1 and C2 using the pure spectra of yeastolate and BSA, respectively.  $\lambda_{ex}/\Delta\lambda$  represents the excitation wavelength and offset of maximum fluorescence intensity.

model better explained the data. The first two components were yeastolate and BSA emission respectively (Table 1), with the high anisotropy of component 2 (Table S5, SI) confirming this assignment. The explained variance for the BSA component in TSFS<sub>||</sub> data was dramatically larger (~44%) than for TSFS<sub>T</sub>. The third component (2-3%) has its maximum excitation peak red shifted from 282 to 290 nm and was stronger in TSFS<sub>||</sub> spectra suggesting that it originated from BSA (Figures S9-11, SI). This could be due to yeastolate components binding to BSA, and thus changing the emission properties, identifying specific binding processes is not feasible due to the large number of potential interactions (e.g. BSA can interact with vitamin B12 and B6 (Zhang et al., 2008), both are present in yeastolate (Mosser et al., 2015). The fourth component (1%-2%) is weaker in the TSFS<sub>||</sub> data which might suggest that this originates from smaller yeastolate fluorophores. The best explanation at the moment is that this represents an IFE based effect where the increased light absorption by BSA as its concentration increases. These MCR identified factors will potentially introduce non-linearities into protein quantification regression models for complex media.

### 3.4 | Model performance

For all models, the optimum number of LVs required was four and these had similar attributions as above. For example, PLS loadings plots of TSFS<sub>||</sub> measurements (Figure 2), where the first LV (99.58% of the variance explained) could be interpreted as the yeastolate contribution, whereas the second LV (0.39% explained variance) could be attributed to BSA emission. The remaining two LVs (~0.02% explained variance) may represent complex species arising from the binding or interaction of yeastolate components with BSA to as suggested by MCR. LVs 2-4 account only for <0.5% of explained variance because the yeastolate concentration is much greater (at least  $\times 10$  that of BSA) and it contains far more small molecule fluorophores. Protein emission is further reduced because of quenching leading to the low explained variance from protein associated sources (i.e., changing concentration, IFE, binding to yeastolate components). Table 2 shows the statistical PLS model performance parameters for the various pTSFS and aniso-TSFS measurements after appropriate pre-processing. Model quality was assessed by

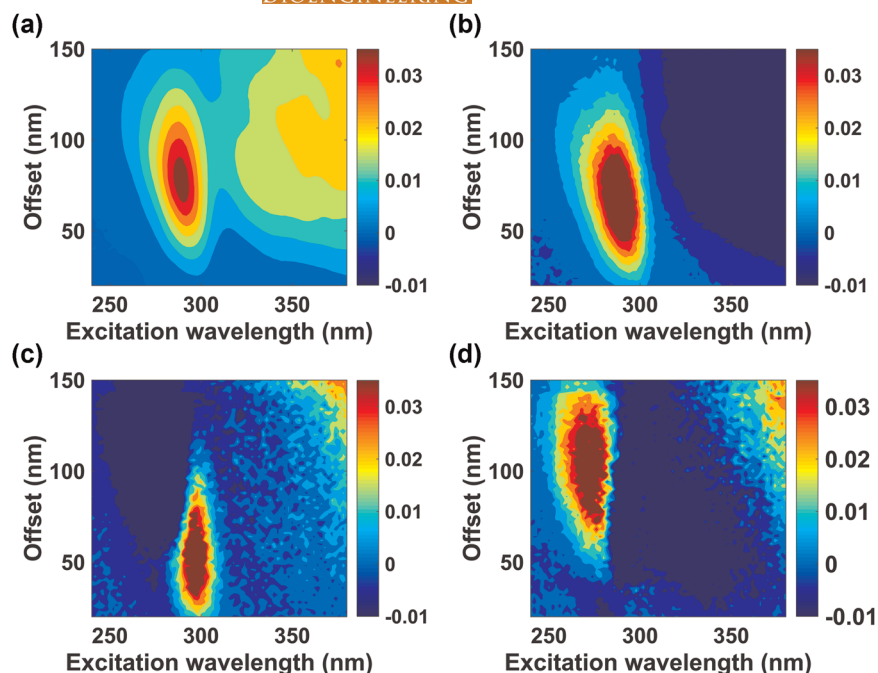


**FIGURE 2** Loadings plots from the PLS regression model built using the TSFS<sub>||</sub> normalized data: (a) LV 1 (99.6% spectral variance explained), (b) LV 2 (0.4% spectral variance explained), (c) LV 3 (0.01% spectral variance explained), and (d) LV 4 (0.01% spectral variance explained). PLS, partial least square; TSFS, total synchronous fluorescence spectroscopy; LV, latent variable [Color figure can be viewed at [wileyonlinelibrary.com](http://wileyonlinelibrary.com)]

**TABLE 2** Statistical parameters of the PLS model performance built using pTSFS and *aniso*-TSFS data

MDF method	Measurement conditions	Calibration set (C-Set)				Test set (T-Set)		
		Calibration RMSEC (g L <sup>-1</sup> )	R <sup>2</sup>	Validation RMSECV (g L <sup>-1</sup> )	R <sup>2</sup> CV	Prediction RMSEP (g L <sup>-1</sup> )	R <sup>2</sup>	REP (%)
TSFS <sub>  </sub>	High resolution (2 nm)	0.06	0.95	0.12	0.84	0.08	0.76	11.6
	GA Selected	0.04	0.99	0.07	0.95	0.07	0.82	10.0
	4 nm resolution	0.06	0.95	0.11	0.84	0.08	0.76	11.9
	<b>Optimized</b>	<b>0.06</b>	<b>0.95</b>	<b>0.12</b>	<b>0.83</b>	<b>0.06</b>	<b>0.94</b>	<b>8.9</b>
TSFS <sub>⊥</sub>	High resolution (2 nm)	0.06	0.96	0.15	0.76	0.08	0.76	11.5
	GA Selected	0.04	0.98	0.10	0.93	0.09	0.77	12.4
	4 nm resolution	0.06	0.96	0.14	0.78	0.08	0.75	11.9
TSFS <sub>T</sub>	High resolution (2 nm)	0.07	0.95	0.12	0.83	0.09	0.73	12.4
	GA Selected	0.04	0.98	0.07	0.95	0.07	0.82	10.7
	4 nm resolution	0.07	0.94	0.12	0.83	0.09	0.72	12.8
<i>aniso</i> -TSFS	Full range (2 nm)	0.05	0.97	0.34	0.00	0.15	0.30	20.7

Note: All models used four LVs and pTSFS data were pre-processed by normalization to maximum intensity. No spectral pretreatment was used for the *aniso*-TSFS data. The best method is highlighted in bold.

Abbreviations: MDF, multidimensional fluorescence; PLS, partial least square; pTSFS, polarized total synchronous fluorescence spectroscopy; REP, relative error of prediction; RMSEC, root-mean-square error of calibration; RMSECV, root-mean-square error of cross-validation, RMSEP, root-mean-square error of prediction.

figures of merit such as the RMSEC, RMSECV, and RMSEP as well as the determination coefficient ( $R^2$ ). Considering the full spectral map using 2 nm spectral resolution, there were no significant differences between the different intensity based pTSFS models. *aniso*-TSFS was worse because of increased noise, and the increase of ~1.4 in REP% agrees with error propagation theory. This is also seen in the EJCR plots (Figure 3a), where it shows an accuracy bias and lower precision compared to the other measurement methods. This confirms the unsuitability of the more complex *aniso*-TSFS based method due to

the larger errors associated with anisotropy calculations, however, the *aniso*-TSFS plots do provide a valuable insight into understanding sample emission properties which can help validate the basis for regression modelling of pTSFS data. Using full MDF measurements to build chemometric models, however, is not optimal because of the high degree of collinearity in this type of data. This means that many variables are redundant and contribute to making the predictive models less reliable. Therefore, one needs to reduce the number of variables to only those that are informative (B. Li et al., 2014).

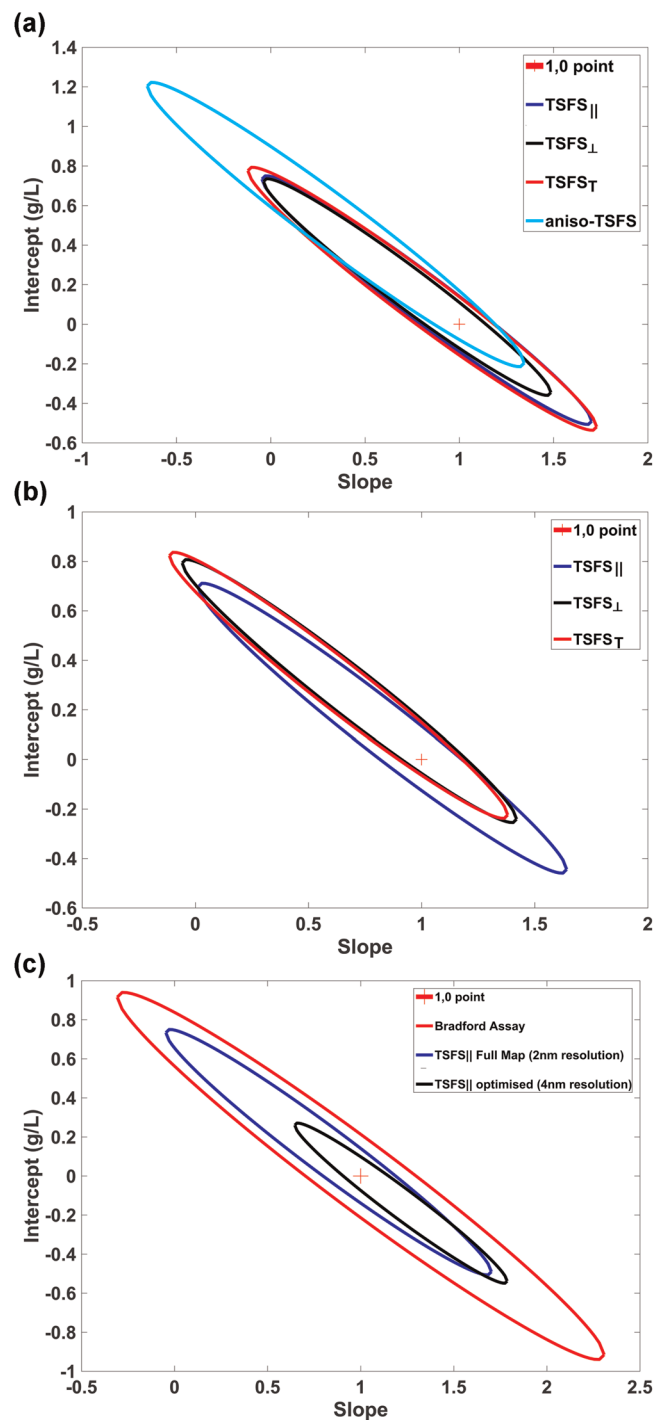


**FIGURE 3** Elliptical joint confidence regions (at 95% level) for the slope and intercept of the PLS pTSFS regression models using: (a) full spectra; (b) GA selected variables, and (c) TSFS<sub>||</sub> full spectra (2 nm resolution), TSFS<sub>||</sub> SNR optimized at 4 nm resolution, and Bradford Assay. PLS, partial least square; pTSFS, polarized total synchronous fluorescence spectroscopy; SNR, signal to noise ratio [Color figure can be viewed at [wileyonlinelibrary.com](http://wileyonlinelibrary.com)]

We expected that this would enable us to refine and shorten the pTSFS data collection method to reduce measurement time. VIP scores is a simple, fast, popular variable selection method available in most commercial software (Farres et al., 2015). Generally, VIP

scores > 1 are used as a criterion for variable selection (Chong & Jun, 2005; Farres et al., 2015), however this cut-off threshold needs to be evaluated for optimal results. Here, selecting variables with VIP scores > 2 were found to improve accuracy by ~10% compared to the full pTSFS spectra. Using lower (>1) or higher (>3) thresholds yielded poorer prediction performance (Table S7, SI) probably because at higher thresholds, the selected variables were being concentrated in the BSA emission region only (Figure S12D–F, SI). This agrees with the MCR analysis that indicated secondary protein effects (LV3 and LV4) were important and that using only protein emission spectral changes was not appropriate.

Using GA variable selection provided a slight improvement (~15%) in prediction accuracy (Table 2) for TSFS<sub>||</sub> based models. However, both GA and VIP-based methods selected variables were distributed across the emission space and as such were less suited for PAT implementation and requires too many excitation wavelengths. We then used iPLS to do variable selection, as this was expected to generate selected variables which has fewer 2D spectra. iPLS did not considerably improve pTSFS models accuracy, but it produced models of equivalent accuracy with six or ten excitation wavelengths: 256, 260, 264, 270, 280, 290, 292, 298, 300 and 364 nm (Figure S12B, Tables S8–9, SI). As with VIP, the selected wavelengths included both long ( $\lambda_{\text{ex}} > 360$  nm) and short ( $\lambda_{\text{ex}} < 300$  nm) wavelength regions. Among the intensity-based methods, the lowest errors of prediction (~10% REP) were obtained for TSFS<sub>||</sub> (Table S7, SI), which proved to be more robust than the other pTSFS methods when iPLS variable selection was applied.

The TSFS<sub>||</sub> model EJCRCs showed that the ideal value (1,0) was located in a more central position (Figure 3b), indicating a lower bias value compared to the other pTSFS models. Of more significance was that only ~25% of the original spectral variables were needed (~1200 from 4686) which were evenly distributed across the spectrum in such a way that their selection could be associated with the minimum spectral resolution required (Figure S12C, SI). This suggested that that using a lower 4 nm resolution would not compromise model quality and also reduce measurement time. This was verified by manually selecting the data in 4 nm steps (in both excitation and emission) and then evaluating the performance of these reduced variables PLS models (Table 2). The results were not significantly different ( $p > .05$ , randomization test) proving that measurement time could be reduced by ~70% (from ~40 to ~8–12 min). The speed improvement will also enable spectral averaging, improving SNR, and thus prediction accuracy.

### 3.5 | Instrument optimization

pTSFS measurement settings used were based on historical values and we needed to validate if these were the optimal instrumental settings for producing single scan spectra with the best SNR, and consequently, the lowest measurement error. Spectral averaging should be an included variable here but was impractical with the current data acquisition speed. SNR optimization of TSFS<sub>||</sub> measurements via instrumental settings was implemented using a

compact Box Behnken design (Table S10, SI) with three parameters: scan rate (120–2400 nm/min), PMT voltage (600–700 V), and emission slit width (2.5 to 10 nm). The highest SNR (5732) was observed for BSA/YST concentrations of 1.2/10 g L<sup>-1</sup> using scan rate of 1200 nm min<sup>-1</sup>, PMT voltage of 650 V and emission bandwidth of 5 nm, although using the same settings for a low BSA concentration yields a poorer SNR. Increasing the excitation slit width is the easiest way to significantly increase fluorescence intensity and hence SNR, but it also increases the amount of scattered and stray light being generated which is a major problem with intrinsic emission measurements. Furthermore, this optimization process is limited by the detector dynamic range (Wiberg et al., 2004), therefore, in this design, the excitation slit was fixed at 10 nm to avoid detector saturation issues. From the ANOVA results, the scan rate and emission bandwidth were most significant at the higher BSA concentrations whereas the scan rate, PMT voltage, and the emission bandwidth were all significant for the lower BSA concentrations (Table S11, SI). Among these, emission bandwidth was the most significant factor ( $p = .001$ ), increasing both SNR responses without reducing accuracy of protein prediction (vide infra). This indicated that spectral resolution was not overly important. At low protein concentrations, the matrix effect was significantly higher, as expected, leading to poorer SNR.

Instrumental optimization was further assessed using the composite desirability function (Figure S13, SI), which provides an overall assessment of how the instrumental settings affected SNR. The optimal solution was found to be: scan rate 600 nm min<sup>-1</sup>, PMT voltage 650 V, and emission slit 8 nm with a composite desirability of 0.99. To make the optimal solution compatible with experimental conditions, the emission slit was set to 10 nm. However, a 600 nm min<sup>-1</sup> scan rate was considered too slow and increased to 1200 nm min<sup>-1</sup>. The composite desirability reduced slightly to 0.84, but this instrumentally optimized TSFS<sub>||</sub> model improved in prediction accuracy (25% RMSEP) compared to the model without instrumental optimization (Table 2). The results of this exercise showed that model accuracy could be substantially improved but also that SNR could not be significantly improved by modifying the instrumental parameters under single scan conditions. This then means that the only option to improve pTSFS measurement SNR on these types of sample is to use spectral averaging. However, with scanning-based fluorometers that is not a particularly viable option, even with the reduced measurement time resulting in using a larger 4 nm step size. The Bradford Assay and EJCR plots (Figure 3c) were used to quickly visualize differences in the accuracy and precision of both methods. This showed that the 1.0 point was located within both ellipses, implying that both methods were accurate. However, ellipse sizes indicated that TSFS<sub>||</sub> was more precise than the Bradford Assay, particularly for optimized TSFS<sub>||</sub> data, which was supported by the figures of merit (Table 3). The TSFS<sub>||</sub> method was clearly superior in terms of sensitivity (LOD and LOQ reduced by ~18% and 28%) and accuracy (~5% REP lower for TSFS<sub>||</sub> method), and dramatically better in terms of predicting new, test, samples. This is explained by the fact that the Bradford Assay is less able to handle interferences arising from the media matrix, and has a limited linear range (Walker, 1996).

**TABLE 3** Comparison of quantification performance and analytical figures of merit for Bradford Assay and optimized TSFS<sub>||</sub> method

	Bradford assay			Optimized TSFS <sub>  </sub> method		
	R <sup>2</sup>	RMSE (g L <sup>-1</sup> )	REP (%)	R <sup>2</sup> Pred	RMSE (g L <sup>-1</sup> )	REP (%)
Calibration	0.93	0.09	11.2	0.95	0.06	9.0
Test	0.67	0.11	13.8	0.94	0.06	8.9
Figures of merit						
LOD (g L <sup>-1</sup> )	0.22			0.18		
LOQ (g L <sup>-1</sup> )	0.75			0.54		

Note: R<sup>2</sup> = coefficient of determination, RMSE = root-mean-square error in g L<sup>-1</sup>, REP = relative error of prediction in %. LOD and LOQ were calculated as the ratio between 3.3 and 10 times the standard deviation of the intercept and the slope of the regression, respectively (ICH Guideline, 2005).

## 4 | CONCLUSIONS

We have demonstrated the potential for pTSFS measurements as a rapid, spectroscopic methodology for potential online or at-line bioreactor monitoring using a model protein-media system. High-resolution pTSFS measurements are time-consuming (~40 min per sample) and for online applications, data acquisition speed needs to be much faster and thus variable selection was employed to see how much the spectra could be reduced. GA variable selection analysis showed that spectral resolution could be safely reduced from 2 to 4 nm without degrading model accuracy which reduced measurement time by 60%. iPLS variable selection further showed that fewer excitation wavelengths (15%) could be used to build models with similar performance to those using full pTSFS spectra. This is a demonstration of the most effective use of variable selection for chemometric modelling, namely the intelligent de-resolving of complex high-resolution measurements (e.g., full TSFS spectra) into simpler datasets which can be acquired using simpler and faster measurement methods.

Further improvement in model performance requires better quality data and specifically higher SNR. Optimization of the instrument measurement using DoE was effective at improving measurement SNR somewhat and reducing model error for these single scan-based experiments. It also showed that reducing scan speed was very significant because it increases the exposure time at each spectral point leading to stronger signals. Unfortunately, this also increases the data acquisition time making the measurement too time consuming (>10 min per spectrum) for off- or at-line measurements. A more practical solution is to use multichannel spectrometers which can both use longer exposure times and undertake spectral averaging without making the overall measurement time too long.

TSFS<sub>||</sub> was found to be best for measuring protein concentration because these spectra had improved protein signal SNR due to the anisotropic protein emission. This better discrimination of the analyte signal from the strong background emission of all the small molecule fluorophores in the cell culture media is the significant

benefit compared to unpolarized MDF measurements resulting in lower predictive errors and higher precision. It also means that only a single spectral measurement is required making the pTSFS method sufficiently fast (<3.5 min) for online/at-line measurements. The optimized TSFS<sub>||</sub>-based measurement method outperformed the Bradford Assay having an LOD of 0.18 g L<sup>-1</sup> and high accuracy with predictive error of less than 10%. In addition, it requires no reagent use or significant sample handling. Another advantage of MDF measurements and thus TSFS<sub>||</sub> is the potential to quantify two or more proteins simultaneously (Wiberg et al., 2004) and the potential to build models for other nonfluorescent bioprocess components like as glucose and ammonia concentration (Ohadi et al., 2014).

The next stage in the development of this pTSFS methodology will focus on the analysis of both real bioprocess cell culture broth samples to demonstrate efficacy with real industrial samples and second on a more complex monoclonal antibody (mAb) spiked protein-media solutions to demonstrate the potential for quantifying mAbs in the presence of other proteins, and this will facilitate the development of the measurement method into a valid PAT tool for upstream bioprocess monitoring.

## ACKNOWLEDGMENTS

This publication emanated from research supported in part by a research grant from Science Foundation Ireland (SFI) and is co-funded under the European Regional Development Fund under Grant number (14/IA/2282, Advanced Analytics for Biological Therapeutic Manufacture, to AGR). We also thank Agilent Technologies (Mulgrave Victoria, Australia) for an instrument loan. The authors declare no financial or commercial conflict of interest.

## AUTHOR CONTRIBUTIONS

Bernard Boateng: *designed and performed the experiments, analyzed the data, prepared all the figures, wrote the original draft, edited the manuscript.* Saioa Elcoroaristizabal: *analyzed data and edited the manuscript.* Alan Ryder: *conceptualization, supervision, funding acquisition, wrote the manuscript.*

## DATA AVAILABILITY STATEMENT

The data that support the findings of this study are available from the corresponding author upon reasonable request.

## ORCID

Bernard O. Boateng  <https://orcid.org/0000-0002-4804-3187>

Saioa Elcoroaristizabal  <https://orcid.org/0000-0001-8374-8302>

Alan G. Ryder  <http://orcid.org/0000-0002-3133-4340>

## REFERENCES

- Anderson-Cook, C. M., Borror, C. M., & Montgomery, D. C. (2009). Response surface design evaluation and comparison. *Journal of statistical planning and inference*, 139(2), 629–641. <https://doi.org/10.1016/j.jspi.2008.04.004>
- Bradford, M. M. (1976). A rapid and sensitive method for the quantitation of microgram quantities of protein utilizing the principle of protein-dye binding. *Analytical Biochemistry*, 72(1), 248–254. [https://doi.org/10.1016/0003-2697\(76\)90527-3](https://doi.org/10.1016/0003-2697(76)90527-3)
- Buckley, K., & Ryder, A. G. (2017). Applications of Raman spectroscopy in biopharmaceutical manufacturing: A short review. *Applied Spectroscopy*, 71(6), 1085–1116. <https://doi.org/10.1177/0003702817703270>
- Calvet, A., Li, B. Y., & Ryder, A. G. (2014). A rapid fluorescence based method for the quantitative analysis of cell culture media photo-degradation. *Analytica Chimica Acta*, 807, 111–119. <https://doi.org/10.1016/j.aca.2013.11.028>
- Casamayou-Boucau, Y., & Ryder, A. G. (2017). Extended wavelength anisotropy resolved multidimensional emission spectroscopy (ARMES) measurements: Better filters, validation standards, and Rayleigh scatter removal methods. *Methods Appl Fluoresc*, 5(3), 037001. <https://doi.org/10.1088/2050-6120/aa7763>
- Casamayou-Boucau, Y., & Ryder, A. G. (2018). Accurate anisotropy recovery from fluorophore mixtures using multivariate curve resolution (MCR). *Analytica Chimica Acta*, 1000, 132–143. <https://doi.org/10.1016/j.aca.2017.11.031>
- Casamayou-Boucau, Y., & Ryder, A. G. (2020). Quantitative analysis of weakly bound insulin oligomers in solution using polarized multidimensional fluorescence spectroscopy. *Analytica Chimica Acta*, 1138, 18–29. <https://doi.org/10.1016/j.aca.2020.09.007>
- Cervera, A. E., Petersen, N., Lantz, A. E., Larsen, A., & Gernaey, K. V. (2009). Application of near-infrared spectroscopy for monitoring and control of cell culture and fermentation. *Biotechnology Progress*, 25(6), 1561–1581. <https://doi.org/10.1002/btpr.280>
- Chiappini, F. A., Teglia, C. M., Forno, Á. G., & Goicoechea, H. C. (2020). Modelling of bioprocess non-linear fluorescence data for at-line prediction of etanercept based on artificial neural networks optimized by response surface methodology. *Talanta*, 210, 120664. <https://doi.org/10.1016/j.talanta.2019.120664>
- Chong, I. G., & Jun, C. H. (2005). Performance of some variable selection methods when multicollinearity is present. *Chemometrics and Intelligent Laboratory Systems*, 78(1-2), 103–112. <https://doi.org/10.1016/j.chemolab.2004.12.011>
- Chutipongtanate, S., Watcharatanyatip, K., Homvises, T., Jaturongkakul, K., & Thongboonkerd, V. (2012). Systematic comparisons of various spectrophotometric and colorimetric methods to measure concentrations of protein, peptide and amino acid: Detectable limits, linear dynamic ranges, interferences, practicality and unit costs. *Talanta*, 98, 123–129. <https://doi.org/10.1016/j.talanta.2012.06.058>
- Classen, J., Aupert, F., Reardon, K. F., Solle, D., & Scheper, T. (2017). Spectroscopic sensors for in-line bioprocess monitoring in research and pharmaceutical industrial application. *Analytical and Bioanalytical Chemistry*, 409(3), 651–666. <https://doi.org/10.1007/s00216-016-0068-x>
- van der Voet, H. (1994). Comparing the predictive accuracy of models using a simple randomization test. *Chemometrics and Intelligent Laboratory Systems*, 25(2), 313–323. [https://doi.org/10.1016/0169-7439\(94\)85050-X](https://doi.org/10.1016/0169-7439(94)85050-X)
- Derringer, G., & Suich, R. (1980). Simultaneous optimization of several response variables. *Journal of Quality Technology*, 12(4), 214–219. <https://doi.org/10.1080/00224065.1980.11980968>
- Despagne, F., Massart, D. L., & Chabot, P. (2000). Development of a robust calibration model for nonlinear in-line process data. *Analytical Chemistry*, 72(7), 1657–1665. <https://doi.org/10.1021/ac991076k>
- Elcoroaristizabal, S., Bro, R., García, J. A., & Alonso, L. (2015). PARAFAC models of fluorescence data with scattering: A comparative study. *Chemometrics and Intelligent Laboratory Systems*, 142(Suppl C), 124–130. <https://doi.org/10.1016/j.chemolab.2015.01.017>
- Faassen, S. M., & Hitzmann, B. (2015). Fluorescence spectroscopy and chemometric modeling for bioprocess monitoring. *Sensors*, 15(5), 10271–10291. <https://doi.org/10.3390/s150510271>
- Farres, M., Platikanov, S., Tsakovski, S., & Tauler, R. (2015). Comparison of the variable importance in projection (VIP) and of the selectivity ratio (SR) methods for variable selection and interpretation. *Journal of Chemometrics*, 29(10), 528–536. <https://doi.org/10.1002/cem.2736>

- Flecha, F. L. G., & Levi, V. (2003). Determination of the molecular size of BSA by fluorescence anisotropy. *Biochemistry and Molecular Biology Education*, 31(5), 319–322. <https://doi.org/10.1002/bmb.2003.494031050261>
- Geladi, P. (2002). Some recent trends in the calibration literature. *Chemometrics and Intelligent Laboratory Systems*, 60(1), 211–224. [https://doi.org/10.1016/S0169-7439\(01\)00197-6](https://doi.org/10.1016/S0169-7439(01)00197-6)
- Ghisaidoobe, A. B. T., & Chung, S. J. (2014). Intrinsic tryptophan fluorescence in the detection and analysis of proteins: A focus on forster resonance energy transfer techniques. *International Journal of Molecular Sciences*, 15(12), 22518–22538. <https://doi.org/10.3390/ijms151222518>
- Graf, A., Classen, J., Solle, D., Hitzmann, B., Rebner, K., & Hoehse, M. (2019). A novel LED-based 2D-fluorescence spectroscopy system for in-line monitoring of Chinese hamster ovary cell cultivations—Part I. *Engineering in Life Sciences*, 19(5), 352–362. <https://doi.org/10.1002/elsc.201800149>
- Gronemeyer, P., Ditz, R., & Strube, J. (2014). Trends in upstream and downstream process development for antibody manufacturing. *Bioengineering (Basel)*, 1(4), 188–212. <https://doi.org/10.3390/bioengineering1040188>
- Groza, R. C., Calvet, A., & Ryder, A. G. (2014). A fluorescence anisotropy method for measuring protein concentration in complex cell culture media. *Analytica Chimica Acta*, 821, 54–61. <https://doi.org/10.1016/j.aca.2014.03.007>
- Haaland, D. M., & Thomas, E. V. (1988). Partial Least-Squares Methods for Spectral Analyses. 1. Relation to other Quantitative Calibration Methods and the Extraction of Qualitative Information. *Analytical Chemistry*, 60(11), 1193–1202. <https://doi.org/10.1021/ac00162a020>
- Hakemeyer, C., Strauss, U., Werz, S., Folque, F., & Menezes, J. C. (2013). Near-infrared and two-dimensional fluorescence spectroscopy monitoring of monoclonal antibody fermentation media quality: Aged media decreases cell growth. *Biotechnology Journal*, 8(7), 835–846. <https://doi.org/10.1002/biot.201200355>
- ICH Guideline, I. H. T. (2005). *Validation of analytical procedures: text and methodology Q2 (R1)*. Paper presented at the International conference on harmonization, Geneva, Switzerland.
- Jensen, W. A. (2017). *Response Surface Methodology: Process and Product Optimization Using Designed Experiments* 4th edition. *Journal of Quality Technology*, 49(2), 186–187.
- Jose, G. E., Folque, F., Menezes, J. C., Werz, S., Strauss, U., & Hakemeyer, C. (2011). Predicting Mab Product Yields from Cultivation Media Components, Using Near-Infrared and 2D-Fluorescence Spectroscopies. *Biotechnology Progress*, 27(5), 1339–1346. <https://doi.org/10.1002/btpr.638>
- de Juan, A., Jaumot, J., & Tauler, R. A. (2014). Multivariate curve resolution (MCR). Solving the mixture analysis problem. *Analytical Methods*, 6(14), 4964–4976. <https://doi.org/10.1039/c4ay00571f>
- Lakowicz, J. R. (2006). *Principles of Fluorescence Spectroscopy*. (3rd Edition ed.). New York: Springer. Retrieved from <https://link.springer.com/book/10.1007/978-0-387-46312-4>
- Leardi, R., Seasholtz, M. B., & Pell, R. J. (2002). Variable selection for multivariate calibration using a genetic algorithm: prediction of additive concentrations in polymer films from Fourier transform-infrared spectral data. *Analytica Chimica Acta*, 461(2), 189–200. [https://doi.org/10.1016/S0003-2670\(02\)00272-6](https://doi.org/10.1016/S0003-2670(02)00272-6)
- Lemaitte, P., Cooksey, C. C., Levine, Z. H., Pintar, A. L., Hwang, J., & Allen, D. W. (2016). National Institute of Standards and Technology measurement service of the optical properties of biomedical phantoms: Current status. In (Eds.) Raghavachari, R. & Liang, R., *Design and Quality for Biomedical Technologies IX* (9700 Bellingham: Spie-Int Soc Optical Engineering).
- Li, B., Ray, B. H., Leister, K. J., & Ryder, A. G. (2013). Performance monitoring of a mammalian cell based bioprocess using Raman spectroscopy. *Analytica Chimica Acta*, 796(0), 84–91. <https://doi.org/10.1016/j.aca.2013.07.058>
- Li, B., Ryan, P. W., Ray, B. H., Leister, K. J., Sirimuthu, N. M. S., & Ryder, A. G. (2010). Rapid Characterization and Quality Control of Complex Cell Culture Media Solutions Using Raman Spectroscopy and Chemometrics. *Biotechnology and Bioengineering*, 107(2), 290–301. <https://doi.org/10.1002/bit.22813>
- Li, B., Ryan, P. W., Shanahan, M., Leister, K. J., & Ryder, A. G. (2011). Fluorescence excitation-emission matrix (EEM) spectroscopy for rapid identification and quality evaluation of cell culture media components. *Applied Spectroscopy*, 65(11), 1240–1249. <https://doi.org/10.1366/11-06383>
- Li, B., Shanahan, M., Calvet, A., Leister, K. J., & Ryder, A. G. (2014). Comprehensive, quantitative bioprocess productivity monitoring using fluorescence EEM spectroscopy and chemometrics. *Analyst*, 139(7), 1661–1671. <https://doi.org/10.1039/c4an00007b>
- Li, B. Y., Sirimuthu, N. M. S., Ray, B. H., & Ryder, A. G. (2012). Using surface-enhanced Raman scattering (SERS) and fluorescence spectroscopy for screening yeast extracts, a complex component of cell culture media. *Journal of Raman Spectroscopy*, 43(8), 1074–1082. <https://doi.org/10.1002/jrs.3141>
- Mandel, J., & Linning, F. J. (1957). Study of accuracy in chemical analysis using linear calibration curves. *Analytical Chemistry*, 29(5), 743–749. <https://doi.org/10.1021/ac60125a002>
- Melcher, M., Scharl, T., Spangl, B., Luchner, M., Cserjan, M., Bayer, K., & Striedner, G. (2015). The potential of random forest and neural networks for biomass and recombinant protein modeling in *Escherichia coli* fed-batch fermentations. *Biotechnology Journal*, 10, 1770–1782. <https://doi.org/10.1002/biot.201400790>
- Mosser, M., Kapel, R., Chevalot, I., Olmos, E., Marc, I., Marc, A., & Oriol, E. (2015). Fractionation of yeast extract by nanofiltration process to assess key compounds involved in CHO cell culture improvement. *Biotechnology Progress*, 31(4), 875–882. <https://doi.org/10.1002/btpr.2110>
- Murphy, K. R., Stedmon, C. A., Graeber, D., & Bro, R. (2013). Fluorescence spectroscopy and multi-way techniques. PARAFAC. *Analytical Methods*, 5(23), 6557–6566. <https://doi.org/10.1039/c3ay41160e>
- Naveenraj, S., & Anandan, S. (2013). Binding of serum albumins with bioactive substances—Nanoparticles to drugs. *Journal of Photochemistry and Photobiology C—Photochemistry Reviews*, 14, 53–71. <https://doi.org/10.1016/j.jphotochemrev.2012.09.001>
- Næs, T., Isaksson, T., Fearn, T., & Davies, T. (2002). *A user friendly guide to multivariate calibration and classification*. NIR publications.
- Nørgaard, L., Saudland, A., Wagner, J., Nielsen, J. P., Munck, L., & Engelsen, S. B. (2000). Interval partial least-squares regression (iPLS): A comparative chemometric study with an example from near-infrared spectroscopy. *Applied Spectroscopy*, 54(3), 413–419. <https://doi.org/10.1366/0003702001949500>
- Odman, P., Johansen, C. L., Olsson, L., Germaey, K. V., & Lantz, A. E. (2010). Sensor combination and chemometric variable selection for online monitoring of *Streptomyces coelicolor* fed-batch cultivations. *Applied Microbiology and Biotechnology*, 86(6), 1745–1759. <https://doi.org/10.1007/s00253-009-2412-y>
- Ohadi, K., Aghamohseni, H., Legge, R. L., & Budman, H. M. (2014). Fluorescence-based soft sensor for at situ monitoring of Chinese hamster ovary cell cultures. *Biotechnology and Bioengineering*, 111(8), 1577–1586. <https://doi.org/10.1002/bit.25222>
- Ohadi, K., Legge, R. L., & Budman, H. M. (2015). Intrinsic fluorescence-based at situ soft sensor for monitoring monoclonal antibody aggregation. *Biotechnology Progress*, 31(5), 1423–1432. <https://doi.org/10.1002/btpr.2140>
- Olivieri, A. C. (2018). *Introduction to multivariate calibration: A practical approach*. Springer. Retrieved from <https://www.springer.com/gp/book/9783319970967>
- Rathore, A. S., Bhambure, R., & Ghare, V. (2010). Process analytical technology (PAT) for biopharmaceutical products. *Analytical and*

- Bioanalytical Chemistry*, 398(1), 137–154. <https://doi.org/10.1007/s00216-010-3781-x>
- Rathore, A. S., & Winkle, H. (2009). Quality by design for biopharmaceuticals. *Nature Biotechnology*, 27(1), 26–34. <https://doi.org/10.1038/nbt0109-26>
- Read, E. K., Park, J. T., Shah, R. B., Riley, B. S., Brorson, K. A., & Rathore, A. S. (2010). Process analytical technology (PAT) for biopharmaceutical products: Part I. Concepts and applications. *Biotechnology and Bioengineering*, 105(2), 276–284. <https://doi.org/10.1002/bit.22528>
- Reusch, D., Habegger, M., Falck, D., Peter, B., Maier, B., Gassner, J., Hook, M., Wagner, K., Bonnington, L., Bulau, P., & Wuhrer, M. (2015). Comparison of methods for the analysis of therapeutic immunoglobulin G Fc-glycosylation profiles-Part 2: Mass spectrometric methods. *mAbs*, 7(4), 732–742. <https://doi.org/10.1080/19420862.2015.1045173>
- Ryan, P. W., Li, B., Shanahan, M., Leister, K. J., & Ryder, A. G. (2010). Prediction of cell culture media performance using fluorescence spectroscopy. *Analytical Chemistry*, 82(4), 1311–1317. <https://doi.org/10.1021/Ac902337c>
- Ryder, A. G. (2018). Cell culture media analysis using rapid spectroscopic methods. *Current Opinion in Chemical Engineering*, 22, 11–17. <https://doi.org/10.1016/j.coche.2018.08.008>
- Ryder, A. G., Stedmon, C. A., Harrit, N., & Bro, R. (2017). Calibration, standardization, and quantitative analysis of multidimensional fluorescence (MDF) measurements on complex mixtures (IUPAC Technical Report). *Pure and Applied Chemistry*, 89(12), 1849–1870. <https://doi.org/10.1515/pac-2017-0610>
- Schwab, K., Amann, T., Schmid, J., Handrick, R., & Hesse, F. (2016). Exploring the capabilities of fluorometric online monitoring on chinese hamster ovary cell cultivations producing a monoclonal antibody. *Biotechnology Progress*, 32(6), 1592–1600. <https://doi.org/10.1002/btpr.2326>
- Shukla, A. A., Wolfe, L. S., Mostafa, S. S., & Norman, C. (2017). Evolving trends in mAb production processes. *Bioengineering & Translational Medicine*, 2(1), 58–69. <https://doi.org/10.1002/btm2.10061>
- Skoog, D. A. (1976). *Fundamentals of analytical chemistry* (3rd ed.). New York, London: New York, London: Holt, Rinehart and Winston.
- Smith, P. K., Krohn, R. I., Hermanson, G. T., Mallia, A. K., Gartner, F. H., Provenzano, M. D., Fujimoto, E. K., Goeke, N. M., Olson, B. J., & Klenk, D. C. (1985). Measurement of protein using bicinchoninic acid. *Analytical Biochemistry*, 150(1), 76–85. [https://doi.org/10.1016/0003-2697\(85\)90442-7](https://doi.org/10.1016/0003-2697(85)90442-7)
- Steiner-Browne, M., Elcoroaristizabal, S., & Ryder, A. G. (2019). Using polarized total synchronous fluorescence spectroscopy (pTSFS) with PARAFAC analysis for characterizing intrinsic protein emission. *Chemometrics and Intelligent Laboratory Systems*, 194, 103871. <https://doi.org/10.1016/j.chemolab.2019.103871>
- Teixeira, A. P., Duarte, T. M., Carrondo, M. J. T., & Alves, P. M. (2011). Synchronous fluorescence spectroscopy as a novel tool to enable PAT applications in bioprocesses. *Biotechnology and Bioengineering*, 108(8), 1852–1861. <https://doi.org/10.1002/bit.23131>
- Walker, J. M. (1996). *The protein protocols handbook* (1996). Springer Science & Business Media.
- Wiberg, K., Sterner-Molin, A., & Jacobsson, S. P. (2004). Simultaneous determination of albumin and immunoglobulin G with fluorescence spectroscopy and multivariate calibration. *Talanta*, 62(3), 567–574. <https://doi.org/10.1016/j.talanta.2003.08.024>
- Wold, S., Sjöström, M., & Eriksson, L. (2001). PLS-regression: A basic tool of chemometrics. *Chemometrics and Intelligent Laboratory Systems*, 58(2), 109–130.
- Wold, S., Sjöström, M., & Eriksson, L. (2002). Partial least squares projections to latent structures (PLS) in chemistry. In P. von Ragué Schleyer, N. L. Allinger, T. Clark, J. Gasteiger, P. A. Kollman, H. F. Schaefer & P. R. Schreiner (Eds.), *Encyclopedia of Computational Chemistry*. Wiley. Retrieved from <https://onlinelibrary.wiley.com/doi/abs/10.1002/0470845015.cpa012>
- Zavatti, V., Budman, H., Legge, R., & Tamer, M. (2016). Monitoring of an antigen manufacturing process. *Bioprocess and Biosystems Engineering*, 39(6), 855–869. <https://doi.org/10.1007/s00449-016-1565-1>
- Zhang, H. X., Huang, X., & Zhang, M. (2008). Spectral diagnostics of the interaction between pyridoxine hydrochloride and bovine serum albumin in vitro. *Molecular Biology Reports*, 35(4), 699–705. <https://doi.org/10.1007/s11033-007-9143-x>

## SUPPORTING INFORMATION

Additional Supporting Information may be found online in the supporting information tab for this article.

**How to cite this article:** Boateng BO, Elcoroaristizabal S, Ryder AG. Development of a rapid polarized total synchronous fluorescence spectroscopy (pTSFS) method for protein quantification in a model bioreactor broth. *Biotechnology and Bioengineering*. 2021;118:1805–1817. <https://doi.org/10.1002/bit.27694>